Meteorol. Atmos. Phys. 59, 153–172 (1996)

Meteorology and Atmospheric Physics

Department of Marine, Earth, and Atmospheric Sciences, North Carolina State University, Raleigh, North Carolina, U.S.A.

Structures of Dynamically Unstable Shear Flows and their Implications for Shallow Internal Gravity Waves Part II: Nonlinear Response

Y.-L. Lin

With 9 Figures

Received January 15, 1995
Revised May 5, 1995

Summary

The nonlinear response of a dynamically unstable shear flow with critical level to an initial temperature anomaly is investigated using a nonlinear numerical model. Both nonconstant and constant shear profiles of the basic flow are considered. Effects of the solid lower boundary on the dynamically unstable, nonlinear flow are also studied. It is found that in a dynamically unstable, linear flow with a hyperbolic tangent wind profile, the updraft is tilted upshear. The result in consistent with that of a linear stability model (LC). The upshear tilt can be explained by the Orr mechanism (1907) and the energy argument proposed by LC. In a dynamically unstable, nonlinear flow, the updrafts produced by a sinusoidal initial temperature perturbation are stronger in the lower layer and are more compact and located further apart compared to the corresponding linear flow. In addition, the perturbed wave energy is slightly smaller than the linear case. It is found that the growth rate is smaller during the early stage and much larger during the later stage. For a localized initial temperature perturbation in a dynamically unstable flow, a stronger updraft with two compensated downdrafts are produced. Gravity waves are produced in a dynamically stable flow with both a hyperbolic tangent wind profile and a linear wind profile. For a linear shear flow with Richardson number less than 1/4, the disturbance grows in the early stage and then decays algebraically at later times, similar to that found in other linear theoretical studies. The influence of the solid lower boundary is to suppress the shear instability in a nonlinear flow with a hyperbolic tangent wind profile of $Ri < 1/4$.

1. Introduction

The study of responses of a stably stratified shear flow with a critical level to an imposed thermal forcing helps explain several mesoscale phenomena, such as the generation of clear air turbulence (Maslowe, 1972), the onset and initial growth of moist convection (Chimonas et al., 1980), the generation of internal gravity waves (Smith and Lin, 1982; Lin and Groff, 1988; reviewed in Lin, 1994a, b), and moist convection associated with midlatitude squall lines (Raymond, 1986; Rotunno et al., 1988; Nicholls et al., 1988). Part I of this series of papers (Lin and Chun, 1993; denoted as LC hereafter) has investigated the response of a dynamically unstable shear flow with a critical level to periodic forcing using a linear stability model. They found that in a dynamically unstable flow, the energy equation requires an upshear tilt of the perturbation streamfunction and vertical velocity where U_z is positive. This allows the energy conversion from the basic shear to the growing perturbation wave energy. In this way, the Reynolds stress is negatively correlated with the shear, as found by Orr (1907) and known as Orr mechanism. The linear stability model of Part I (LC) may be applied to investigate the early development of

a squall line if one regards the propagation of a midlatitude squall line as a tropospheric internal gravity wave in a CISK-like process (Raymond, 1984; Cram et al., 1992). However, the disturbance in the real fluid system, such as the atmosphere and ocean, often grows from a localized, finite-amplitude perturbation. Thus, an initial value problem needs to be addressed in order to understand the development of the shallow internal gravity waves generated by an isolated, initial thermal forcing.

Lin and Smith (1986) solved an initial-value problem analytically for a linear, stably stratified hydrostatic, uniform flow with a localized heat source. Nicholls et al. (1991b) also showed that the structure of the propagating disturbances is similar to gravity waves produced in two-dimensional numerical simulations of Florida convection (Nicholls et al., 1991a). It is well recognized (Orr, 1907; Case, 1960a; Pedlosky, 1987) that the discrete normal modes do not form a complete set of the wave spectrum since an arbitrary initial condition cannot be expressed as a sum of discrete normal modes of suitably chosen amplitude due to the neglect of the continuous spectrum of neutral modes. This type of non-model time dependency is typically a complicated mixture of algebraic modulations in amplitude of an oscillatory signal of variable frequency and vertical wavelength (Farrell, 1984). Energy extracted from the basic flow during the initial development of non-modal (algebraic) growth is responsible for exciting the persistent normal mode during the later stage. Examples can be found in the Couette flow (Orr, 1907), internal waves in constant shear flow (Phillips, 1966), Rossby waves in constant shear flow (Yamagata, 1976), and baroclinic waves in the Eady model (Farrell, 1984). An asymptotic solution for a stably stratified flow with constant shear to an initial perturbation has been solved analytically by Case (1960b). It is found that there are an infinite number of discrete eigenvalues plus two continua. After a long time, an initial perturbation becomes a sum of oscillatory terms plus a term which vanishes as $t^{-1/2}$ for $Ri > 1/4$. If $Ri < 1/4$, then there exists either one or zero discrete eigenvalue plus, again, two continua. The latter result is an asymptotic $t^{\mu} - 1/2$, where $\mu = \sqrt{1/4 - Ri}$, behavior for an initial perturbation. The effects of wind shear on the structure and propagation of gravity waves have also been discussed by Lindzen and Tung (1976), Tripoli and Cotton (1989a, b), Crook (1988) and Schmidt and Cotton (1990) among others. In this study, we are particularly interested in the time evolution of wave energy and the nonlinear response in a dynamically unstable atmosphere with a critical level to an initial thermal forcing.

The flow near the critical level in a quasi-steady system is highly nonlinear since a small perturbation in the horizontal velocity field will easily exceed the basic horizontal velocity near the critical level in the reference frame moving with the basic flow. Using a nonlinear numerical model, Breeding (1971) showed that a significant amount of wave energy can be reflected from the critical level for a relatively small value of Richardson number ($Ri < 2.0$), while the response is similar to that of the linear flow for a large Richardson number ($Ri > 2.0$). The theoretical study of Stewartson (1981) with weakly nonlinear effects included in the critical layer showed that the problem is extremely complicated and much remains to be done. An extensive review of linear and weakly nonlinear flows with critical level can be found in Maslowe (1986) and Lindzen (1988). According to the linear theory of Part I (LC), the upshear tilt of updrafts and streamfunction results from the extaction of wave energy associated with the basic shear flow in a dynamically unstable flow. It is essential to investigate the flow structure, energy budget, and momentum flux in the nonlinear regime.

In the real atmosphere, the energy generated by either an initial disturbance or a steady thermal or mechanical forcing should be allowed to radiate out. In linear stability models, such as that developed in Part I (LC), a rigid top boundary is often used. This type of rigid upper boundary has also been adopted by Breeding (1971) in a nonlinear numerical model in studying the flow response to an imposed vorticity source existing at the upper boundary. In this way, the energy generated from the lower layer will be reflected from the upper boundary back to the physical domain and should be considered unrealistic. Thus, an upper boundary condition which allows the energy to propagate away from the physical domain, such as a sponge layer (Klemp and Lilly, 1978) or a radiation boundary condition (Klemp and Durran, 1983; Bougeault, 1983), is needed. Wave reflection from the rigid lower boundary in a uni-

form flow over a prescribed heat source has been shown in several studies (e.g., Smith and Lin, 1982; Lin and Smith, 1986; Raymond, 1986; Bretherton, 1988). The influence of the presence and position of solid boundaries on the stability of an inviscid, stratified shear flow, with a hyperbolic tangent velocity profile and an exponentially decreasing density, was investigated by Einaudi and Lalas (1976). The presence of solid boundaries was shown to stabilize short wavelength and destabilize long wavelength. In this study, we will investigate the influence of the position of the critical level, where in the initial temperature perturbation is located, on the growth rate in a dynamically unstable atmosphere.

The purpose of this study is to investigate the flow response of a stably stratified shear flow with critical level to an initial temperature anomaly using a nonlinear numerical model. The two-dimensional nonlinear model will be presented briefly in Section 2. The results will be discussed in Section 3. The nonlinear flow responses to a periodic temperature perturbation in a dynamically unstable flow will be compared with the results of linear modeling simulations and the linear stability model of Part I (LC). In this way, the nonlinear effects can be studied thoroughly. Both the flow field, energy budget, and momentum flux will be presented and discussed. Then the flow response of a flow with a constant shear to an initial temperature anomaly will be investigated. Flow with both large and small Richardson numbers will be discussed. At last, the lower boundary effects on the flow response will be studied. Concluding remarks are made in the last section.

2. The Nonlinear Numerical Model

In this two-dimensional nonlinear numerical model, we consider the following horizontal momentum equation, hydrostatic equation, incompressible continuity equation, and thermodynamic equation in a nonrotating, Boussinesq fluid,

$$\frac{\partial u}{\partial t}+(U+u)\frac{\partial u}{\partial x}+w\left(U_z+\frac{\partial u}{\partial z}\right)+\frac{1}{\rho_0}\frac{\partial p}{\partial x}=-\nu u, \tag{1}$$

$$\frac{1}{\rho_0}\frac{\partial p}{\partial z}=g\frac{\theta}{\theta_0}, \tag{2}$$

$$\frac{\partial u}{\partial x}+\frac{\partial w}{\partial z}=0, \tag{3}$$

$$\frac{\partial \theta}{\partial t}+(U+u)\frac{\partial \theta}{\partial x}+w\left(\Theta_z+\frac{\partial \theta}{\partial z}\right)=\frac{\theta_0}{c_p T_0}q-\nu\theta, \tag{4}$$

where $U(z)$ and $\Theta(z)$ denote the wind velocity and the potential temperature of the basic flow, q the diabatic heating per unit mass, ν the coefficient of Rayleigh friction and Newtonian cooling, and ρ_0, θ_0, and T_0 are constant reference values. Other symbols have their usual meanings. The flow variables are separated into basic and perturbation parts which are represented by upper and lower cases, respectively. In this study, the Brunt-Vaisala frequency, $N^2=(g/\theta_0)\Theta_z$, is assumed to be constant with height except in the sponge layer (10–15 km) and the diabatic forcing (q) is set to zero.

The major features of numerical schemes used to solve the above system may be briefly summarized in the following:

(i) Leapfrog scheme in time.
(ii) Fourth-order central spatial differencing in horizontal.
(iii) Second-order central spatial differencing in vertical.
(iv) Radiation condition at lateral boundaries (Orlanski, 1976).
(v) Sponge layer on top of the upper boundary of the physical domain (Klemp and Lilly, 1978).
(vi) Fourth-order diffusion or numerical smoother.

In the model calculation, Eqs. (1) and (4) are used to predict the values of u and θ, respectively, for the next time step from the present and last time steps. Equation (3) is then integrated upward to obtain the vertical velocity with the lower boundary conditon specified. Meanwhile, the pressure field is obtained by integrating the hydrostatic equation, Eq. (2), downward. The upper radiation boundary condition is simulated by a sponge layer within which the coefficient of Rayleigh friction and Newtonian cooling is increased from 0 to $5\times10^{-4}\,\mathrm{s}^{-1}$ at the top of the model domain according to the sine square function. A free-slip boundary condition is applied at the lower flat surface. This model has been adopted by Lin and Chun (1991) and Lin et al. (1993) for studying the generation mechanism of density currents in a shear flow with critical level over a prescribed cooling region. A more detailed

Table 1. *Summary of Numerical Experiments*

Case	1A	1B	1C	1E	2A	2C	2D	3A
Figure No.	1	2	3	4	5	6	7	8
Nonlinearity	no	yes	yes	yes	yes	yes	yes	yes
θ_i (.3 K)	periodic	periodic	box	box	box	box	box	box
Wind Profile	tanh	tanh	tanh	tanh	linear	linear	linear	tanh
z_i (km)	5	5	5	5	5	2	2	2
z_1	4	4	4	4	4	1	1	1
z_2	6	6	6	6	6	3	3	3
$N(s^{-1})$	.00237	.00237	.00237	.01	.00168	.00237	.00237	.00237
Shear (s^{-1})	.0075	.0075	.0075	.0075	.0053	.0053	.0053	.0075
(shear layer-km)	(3–7)	(3–7)	(3–7)	(3–7)	(3–7)	(0–4)	(0–2)	(0–4)
Ri	0.1	0.1	0.1	1.8	0.1	0.2	0.2	0.1
Shear Instability	yes	yes	yes	no	no	no	no	very weak

* Other flow parameters: $U_0 = 15\,\mathrm{ms}^{-1}$, $h = 2\,\mathrm{km}$, $b = 25\,\mathrm{km}$. N increases linearly to $0.0237\,\mathrm{s}^{-1}$ at 15 km from the value at 10 km.

description of the model is given in these two papers and in Weglarz (1994).

The vertical model domain is 15 km and the vertical grid interval is 100 m for all cases. The sponge layer extends from 10 to 15 km. The horizontal domain is 200 km and the horizontal grid interval is 5 km. The time step used in all simulations is 5 s. The initial temperature anomaly is prescribed in the vicinity of the critical level either as a periodic function in the horizontal or as a warm bubble with a maximum magnitude of 0.3 K. The structures of these initial temperature anomalies will be described in more detail along with the discussions.

The basic wind has either a hyperbolic tangent profile or a constant shear in the whole layer or in a shallow layer, which are expressed either by

$$U(z) = U_0 \tanh\left(\frac{z - z_i}{h}\right), \tag{5}$$

or

$$U(z) = -U_0 + U_z z, \tag{6}$$

where z_i is the wind reversal level (critical level), h a vertical scale over which the wind shear is large, U_0 the basic wind speed at the surface, and U_z the constant wind shear. With a positive U_0, the basic wind blows from right to left in the lower layer ($z \leqslant z_i$ or $z \leqslant U_0/U_z$) and reverses its direction in the upper layer. Notice that the critical level defined in this study is based on the basic wind velocity.

3. Results

The response of a stratified flow with a hyperbolic tangent vertical shear to an initial temperature perturbation will be presented in Section 3.1. Flows with both small and large Richardson numbers will be studied. The upshear tilt of the updraft and the nonlinear effects will be discussed. The response of a flow with a constant shear will be investigated in Section 3.2. Both deep shear and shallow shear will be considered. In Section 3.3, the influence of the solid lower boundary on the flow stability will be presented. The parameters of these experiments are summarized in Table 1.

3.1 Nonlinear Effects

In order to investigate the nonlinear effects, we perform one linear numerical simulation (Case 1A) of an inviscid flow with a small Richardson number ($Ri < 1/4$) and a hyperbolic tangent wind profile as described by Eq. (5) with $U_0 = 15\,\mathrm{ms}^{-1}$, $z_i = 5\,\mathrm{km}$, and $h = 2\,\mathrm{km}$. The Brunt-Vaisala frequency is assumed to be $0.00237\,\mathrm{s}^{-1}$ in the physical domain ($0 \leqslant z \leqslant 10\,\mathrm{km}$) and increased linearly to $0.0237\,\mathrm{s}^{-1}$ at the top of the sponge layer ($10 < z \leqslant 15\,\mathrm{km}$). Since the shear is concentrated in the layer of $z_i - h$ and $z_i + h$, the Richardson number at z_i is roughly equal to $(Nh/U_0)^2 = 0.1$. The nonlinear terms of Eqs. (1)–(4) are deactivated in this experiment. In this way, it is easier to isolate the nonlinear effects and compare with the results of linear stability model of LC.

Detailed quantitative comparison is impossible because the initial condition is not assumed in the linear stability model. Thus, we will make only qualitative comparisons. The initial temperature perturbation is assumed to have a periodic temperature anomaly as

$$\theta_i = \theta_{i0} \sin\left(\frac{2\pi x}{b}\right) \sin\left[\frac{\pi(z-z_1)}{(z_2-z_1)}\right], \tag{7}$$

where θ_{i0} and b are set to be 0.3 K and 25 km, respectively.

Figure 1 shows the vertical velocity, perturbation horizontal velocity, perturbation pressure, perturbation potential temperature, total streamfunction, momentum flux, and energy budget after 2 h for this control case (Case 1A). The initial temperature perturbation is shown in Fig. 1h. The vertical velocity (Fig. 1a) shows an upshear phase tilt which is required by the energy equation for a growing disturbance in a shear unstable flow (Orr mechanism) as also shown in LC. Near the tropopause (10 km), the phase tilts upstream (left) with height. This feature is different from that of LC because a radiation condition, approximated by a sponge layer, is used in the present model. The addition of the sponge layer allows the disturbance generated from the physical domain ($z \leqslant 10$ km) to propagate upward. The negative momentum flux near the tropopause (Fig. 1f) indeed indicates that an upward energy propagation according to the Eliassen and Palm theorem (1960). The perturbation horizontal velocity and potential temperature fields (Figs. 1b and c) show that both the maxima and minima are located at about 5 km. The actual critical level, based on the sum of basic and perturbation wind velocity, is displaced in the layer of 4 to 6 km. The u field exhibits a downshear tilt in the shear layer (4–6 km), although it is tilted upshear in the whole layer. The vertical velocity and the perturbation horizontal velocity are out of phase by $\pi/2$ in the lower uniform layer and by π in the shear layer and upper uniform layer. As explained in LC, the perturbation horizontal velocity is dominated by the local growth ($\partial u/\partial t$) in the shear layer and by the horizontal advection ($U\partial u/\partial x$) in the lower uniform layer in relation to the vertical velocity, according to the horizontal momentum equation. However, the phase difference (π) in the upper uniform layer is different from that in the stability model ($\pi/2$, LC) since the wave energy is able to propagate out of the upper boundary in the present model. The phase difference (π) between u and w fields in this upper layer is required by the upper radiation boundary condition. The radiation of wave energy is also evidenced by the negative vertical momentum flux (Fig. 1g). Notice that the vertical momentum flux is negatively proportional to the vertical energy flux (Eliassen and Palm, 1960). The vertical orientation in the lowest 2 km is due to the reflection from the surface.

In the shear layer, there exists a downshear tilt for both u and θ fields. These results are similar to the linear stability model results of LC. It is suggested by LC that the downshear tilt of the u and θ fields in the shear layer is due to the local growth ($\partial u/\partial t$ and $\partial\theta/\partial t$) in response to the vertical motion, according to the horizontal momentum equation and the thermodynamic equation, respectively. Both the u and θ fields are also tilted upstream near the tropopause (Figs. 1b and c). Similar to that of LC, the pressure field has an upshear tilt in the layer and is out of phase from the vertical velocity by $\pi/2$ in the shear layer and lower uniform layer (Fig. 1d). This pressure gradient force is responsible for the overturning in the upper layer and the feeding of downdraft air from the front for air parcels flowing in from the right side of the lower layer (Fig. 1e; LC). The potential temperature perturbation is produced by the adiabatic warming and cooling. The cold (warm) region is located at the region of upward (downward) motion where the initial temperature perturbation is positive (negative). The linear stability model of Part I (LC) may be applied to investigate the early development of a squall line if one regards the propagation of a midlatitude squall line as a tropospheric internal gravity wave in a CISK-like process (LC).

As derived by LC, the energy equation is

$$\frac{\partial}{\partial t}\int_0^{z_T} \bar{E}\, dz = -\rho_0 \int_0^{z_T} U_z \overline{uw}\, dz + \left(\frac{g^2\rho_0}{c_p T_0 N^2 \theta_0}\right) \int_0^{z_T} \overline{\theta q}\, dz + \overline{pw}(0) - \overline{pw}(z_T), \tag{8}$$

where the total energy is made up by the kinetic wave energy $(\rho_0/2)u^2$ and the available potential energy $(\rho_0/2)[g\theta/\theta_0 N]^2$. Notice that the w^2 term is ignored in the kinetic wave energy in a hydrostatic atmosphere. The vertical momentum flux is nega-

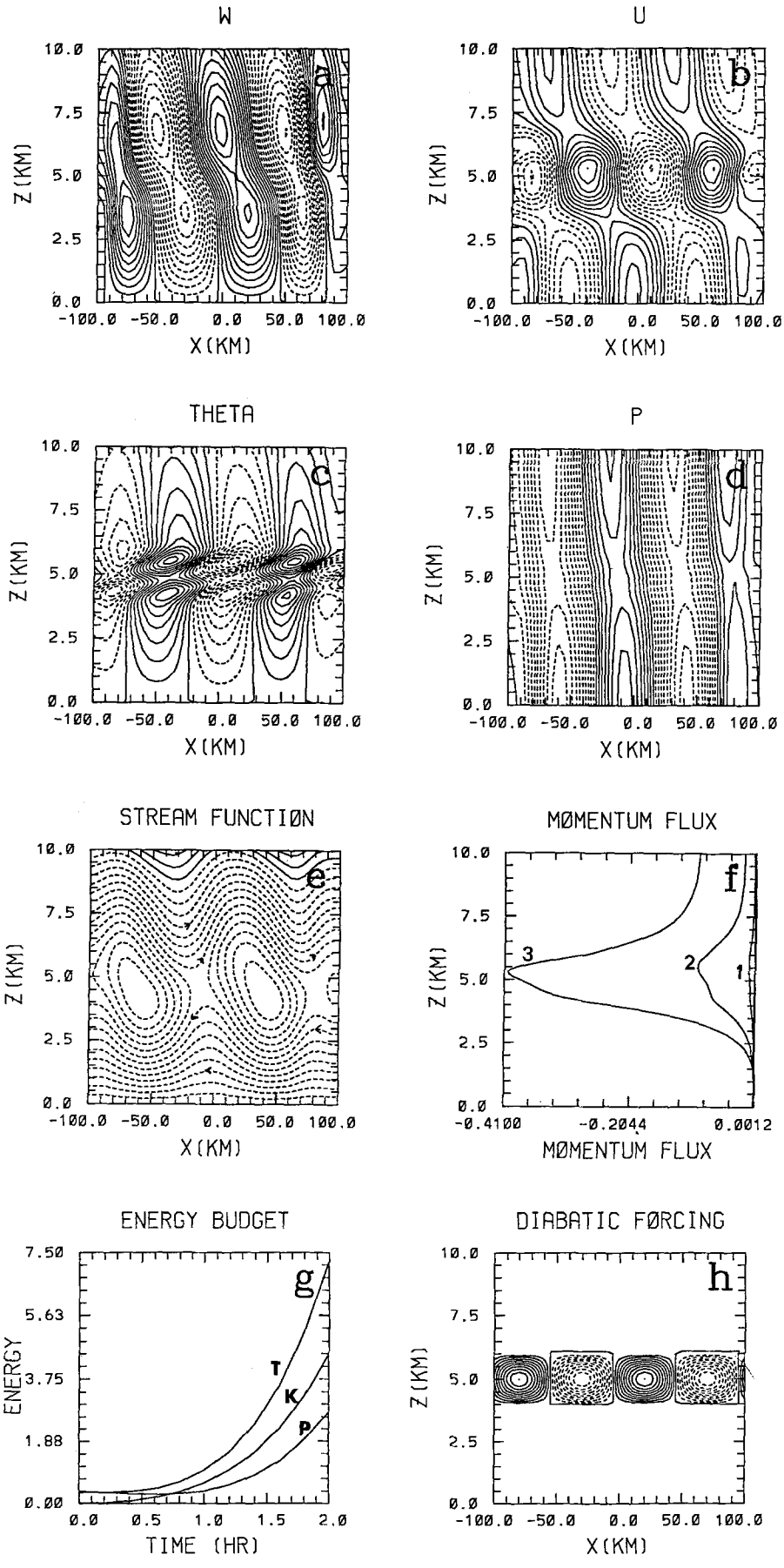

Fig. 1. (Case 1A). (a) Vertical velocity (ms^{-1}), (b) perturbation horizontal velocity (ms^{-1}), (c) perturbation potential temperature (K), (d) perturbation pressure (Pa), (e) total streamfunction, (f) vertical momentum flux, (g) wave energy budget, and (h) initial perturbation temperature for a linear, unstable flow after 2 h. The initial temperature perturbation is described in Eq. (7) with $\theta_{io} = 0.3$ K and b = 25 km. The initial temperature anomaly is confined in the layer of $z_1 = 4$ km to $z_2 = 6$ km. The wind profile is described by a tanh curve and given by Eq. (5) with $U_0 = 15\,ms^{-1}$, $z_i = 5$ km, and $h = 2$ km. Other flow parameters used are $N = 0.00237\,s^{-1}$, and $\theta_{io} = 0.3$ K. The Brunt-Vaisala frequency increases linearly to $0.0237\,s^{-1}$ at $z = 15$ km from $z = 10$ km. The Richardson number near z_i is about 0.1. The total perturbation wave energy, available potential energy, and kinetic energy are denoted by T, P, and K, respectively. There are three time steps depicted in the momentum flux profiles.

tive in the whole domain (Fig. 1f), which provides a positive secondary energy source to the shear unstable flow since U_z is positive. The vertical momentum flux grows much more rapidly in the shear layer due to the shear instability (Eq. (8)). Unlike the stability model of LC, the vertical energy flux at the top boundary (z_T) is positive since the vertical momentum flux is negative there, according to the Eliassen and Palm theorem.

Figure 1g shows the time evolutions of total perturbation wave energy (T), kinetic energy (K), and potential energy (P). Unlike the linear stability model, the initial available potential energy is not zero since the disturbance is triggered by the initial temperature anomaly. The initial kinetic energy is zero since there is no initial motion assumed. The growth of the disturbance is very different from the linear stability model of LC. Evidently, there exist two separate stages of wave development, a very slow growth during the early stage and a rapid growth during the later stage. As mentioned in the introduction, the slow (algebraic) growth during the early stage is due to the continuous spectrum of wave modes, which is responsible for exciting the exponential (modal) growth at later times.

In order to investigate the nonlinear effects, we perform a simulation similar to Case 1A except with the nonlinearity activated (Fig. 2, Case 1B). The maximum vertical velocity is about 0.72 ms^{-1}, which is about the same as that of Case 1A. However, the vertical motion is stronger in the lower layer below 5 km than that in the upper layer. In addition, the updrafts are more compact and located further apart compared to the linear case. This may be explained by the nonlinear effects. For example, let us consider the time evolution of u at $(x, z) = (10, 1\,\text{km})$ in Fig. 1. Since $\partial u/\partial t \propto -u\partial u/\partial x, u$ will increase with time if the nonlinear horizontal advection term (i.e. $-u\partial u/\partial x$) is included in the simulation. Similarly, u will decrease at $(x, z) = (30, 1\,\text{km})$. Therefore, the convergence $(-\partial u/\partial x)$ at $(x, z) = (20, 1\,\text{km})$ will increase at a later time. Due to mass continuity, the updraft will strengthen. This may have some impact on the later development of the disturbance, especially when the atmosphere is moist. The perturbations in the horizontal velocity, potential temperature, pressure, and vorticity fields are weaker than the linear case. In the shear layer, the maxima and minima of the u and θ fields are colocated exactly at the critical level (Figs. 2b and c). This can be seen from that the phase coincidence of the maxima and minima of u and θ fields. The vertical momentum flux shows a similar profile as the linear case, but with a smaller value. This indicates that the vertical velocity is less in phase with the horizontal velocity in a nonlinear flow. The time evolution of the wave energy indicates that the growth of the disturbance is more rapid at earlier stages compared to the linear response, but slows down at later stages.

Since the initial disturbance in the real atmosphere is often observed to be localized, we perform an experiment (Case 1C) with an initial isolated temperature perturbation located in the box of $x = -15$ to 15 km and $z = -4$ to 6 km. The magnitude of the temperature perturbation is 0.3 K, same as previous cases. Figure 3 shows the nonlinear response after 2 h. In general, the results are similar to one cell of the flow in Case 1B. Again, the vertical velocity (Fig. 3a) shows an upshear tilt with two regions of weaker downdraft on both left and right sides. The updraft is stronger in the lower layer below the critical level. Notice that the downdrafts are not produced by the initial cold air as in cases with periodic temperature perturbations. Instead, these are compensating downdrafts accompanying the updraft, which are required by the mass continuity. One of the reasons for examining the response to a localized disturbance is that it is easier to understand the dynamics. The pressure field shows that the upshear tilted low (high) pressure is located to the right (left) side of the updraft. Unlike Case 1B, the low pressure on the upshear side in the lower layer (left side) of the high pressure is very weak. In this way, the pressure gradient is concentrated on the downshear (right) side of the updraft, which gives a much stronger circulation (Fig. 3e). Since the flow is adiabatic, the pressure is directly related to the vertical integration of the temperature (or density) anomaly from above, according to the hydrostatic balance. This can be seen from the potential temperature field (Fig. 3c) which has a general cold air above the surface region of $x = -40$ to 10 km. This area coincides with the surface high pressure region (Fig. 3d). The cold and warm regions are produced respectively by the upward and downward motions adiabatically. In order to investigate the sensitivity to the vertical resolution, a case

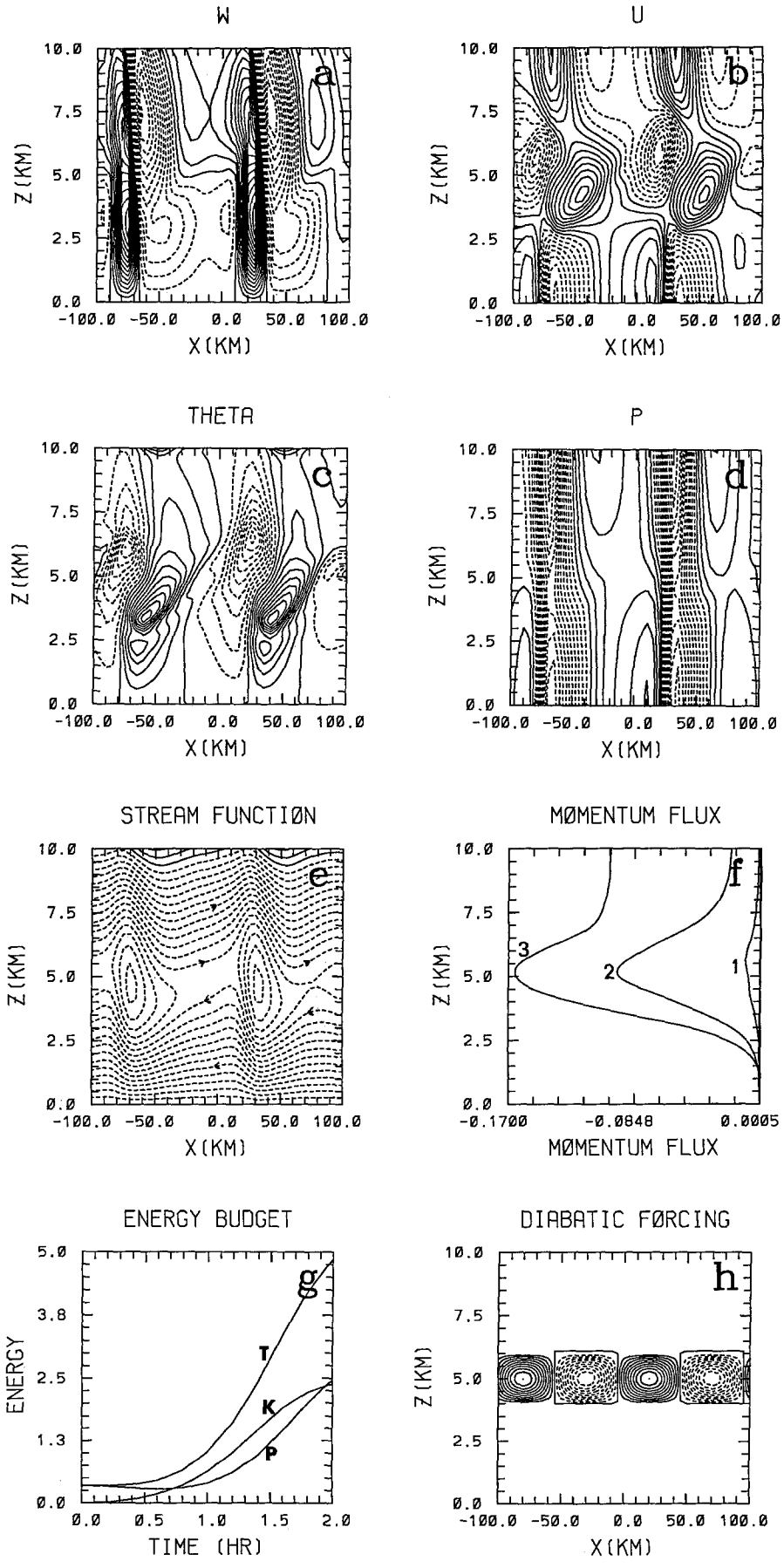

Fig. 2. (Case 1B). Same as Fig. 1 except for a nonlinear flow

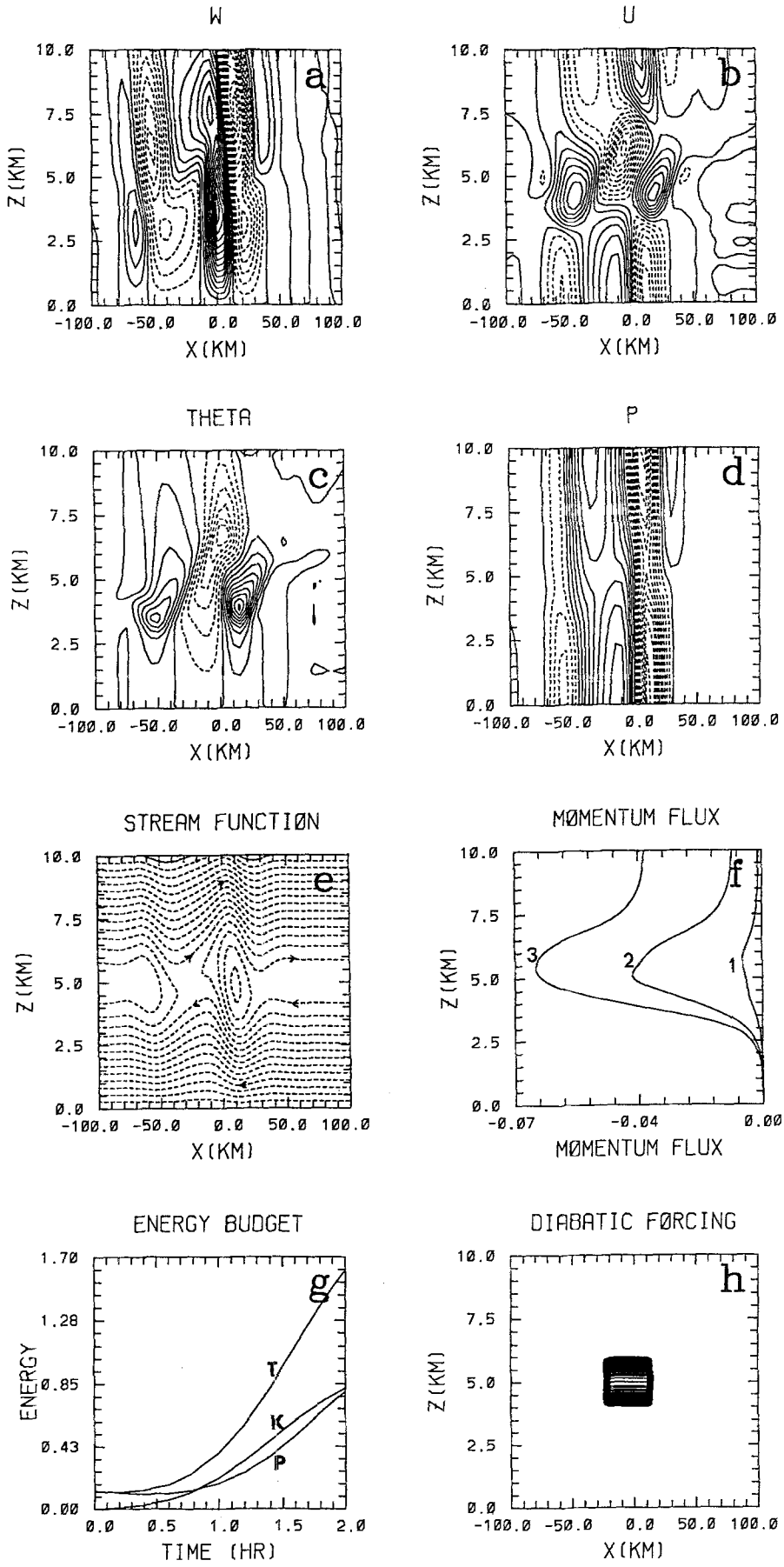

Fig. 3. (Case 1C). Same as Fig. 1 except with the initial temperature perturbation being isolated and a nonlinear flow. The initial temperature perturbation is confined in a box of $x = -15$ to 15 km and $z = -4$ to 6 km

similar to Case 1C is performed with $\Delta z = 20$ m. The result is almost identical (not shown).

In order to investigate the role of shear instability on the flow response, we perform a simulation similar to Case 1C except with $N = 0.01\,s^{-1}$ (Case 1E). This gives a Richardson number of about 1.78 at z_i, so that the flow is expected to be dynamically stable. Figure 4 shows the nonlinear response after 0.5 h. The Brunt-Vaisala frequency in the sponge layer (above 10 km) is linearly increased to $0.0237\,s^{-1}$ at the top. The other parameters are kept the same as those in Case 1C (Fig. 3). The vertical velocity field (Fig. 4a) depicts two regions of updrafts in both upper ($z < 5$ km) and lower layers. These updrafts are propagating away from the center of the initial temperature perturbation. Accompanying these updrafts are weaker compensative downdrafts. The disturbance is a pure gravity wave generated by the initial warm air as also found in the linear theory of a uniform flow over a pulse heating (Lin and Smith, 1986) in which a pulse heating is used. The response of a quienscent fluid to a steady low-level heating (Nicholls et al., 1991a) also indicates both the left- and right-moving updrafts from the heating center are produced. The downshear (to the right in the lower layer) propagating updraft is stronger and travels at a slower speed because it is against the basic flow. The updraft in the upper layer behaves like a jet emitted from the initial perturbation in the upper layer, while it is oriented vertically in the lower layer due to the wave reflection from the surface. This is similar to the response of a quiescent fluid to an initial diabatic heating (Nicholls et al., 1991b). Thus, the asymmetry of the gravity waves in the present case is due to the vertical wind shear. The u field (Fig. 4b) shows a convergence (divergence) at the bottom of the updraft (downdraft) and a divergence (convergence) at the top of the updraft (downdraft). The four-cell pattern near the center of the domain is produced by the strong temperature disturbance (Fig. 4c). The distribution of perturbation pressure is directly related to the temperature perturbations hydrostatically. The warm air located in the layer of 4 to 6 km (Fig. 4c) is associated with the initial temperature perturbation. The upper and lower parts of this warm air are advected by the basic wind. Notice that a cold region is produced in the vicinity of the initial warm air in a dynamically unstable flow (Fig. 3c). Two regions of cold air are present above and below this warm region, which are required by the mass continuity.

The streamfunction field (Fig. 4e) is disturbed only slightly since the flow is dynamically stable. In the vicinity of the critical level, there exists two regions of shallow flow overturning which is similar to that found in Lin (1987). The vertical momentum flux (Fig. 4f) shows an oscillation of the profile in the middle layer. The wave energy remains steady before 0.5 h and then decays linearly afterwards (not shown). The kinetic energy is increasing at the early stage, but the potential energy is decreasing in the whole time period since the system is dynamically stable.

3.2 *Flow with a Constant Shear*

Since a constant shear is often used in many numerical studies of mesoscale convective systems, it is important to investigate the flow response to an initial temperature perturbation in such an environment. The temperature perturbation may be viewed as a warm bubble released initially or the warm region generated by latent heating at later times. Figure 5 shows the nonlinear response of a case (Case 2A) similar to Case 1C except with a constant shear and a simulation time of 3 h. The results may be compared with Case 1C. The initial isolated temperature perturbation (Fig. 5h) is assumed to be the same as Case 1C (Fig. 3h). The Brunt-Vaisala frequency and constant shear (U_z) are $0.00168\,s^{-1}$ and $0.0053\,s^{-1}$, respectively. The level of wind reversal is located at 5 km, which gives a surface wind speed of $-25\,ms^{-1}$. The Richardson number associated with the basic flow is 0.1, which is the same as in Case 1C.

The response is quite different from the case with a tanh wind profile (Case 1C), even though both cases have the same Richardson number of 0.1 in the shear layer. A pair of updraft and downdraft of about equal strength forms near $x = 50$ km (Fig. 5a). Both updraft and downdraft are oriented almost vertically, which are tilted upshear in the nonconstant shear case (Case 1C, Fig. 3a). This indicates that the system at 2 h is not at a growing stage according to the energy argument of LC. In fact, the wave energy evolution does indicate that the system reaches its maximum strength at about $t = 1.75$ h and then decays

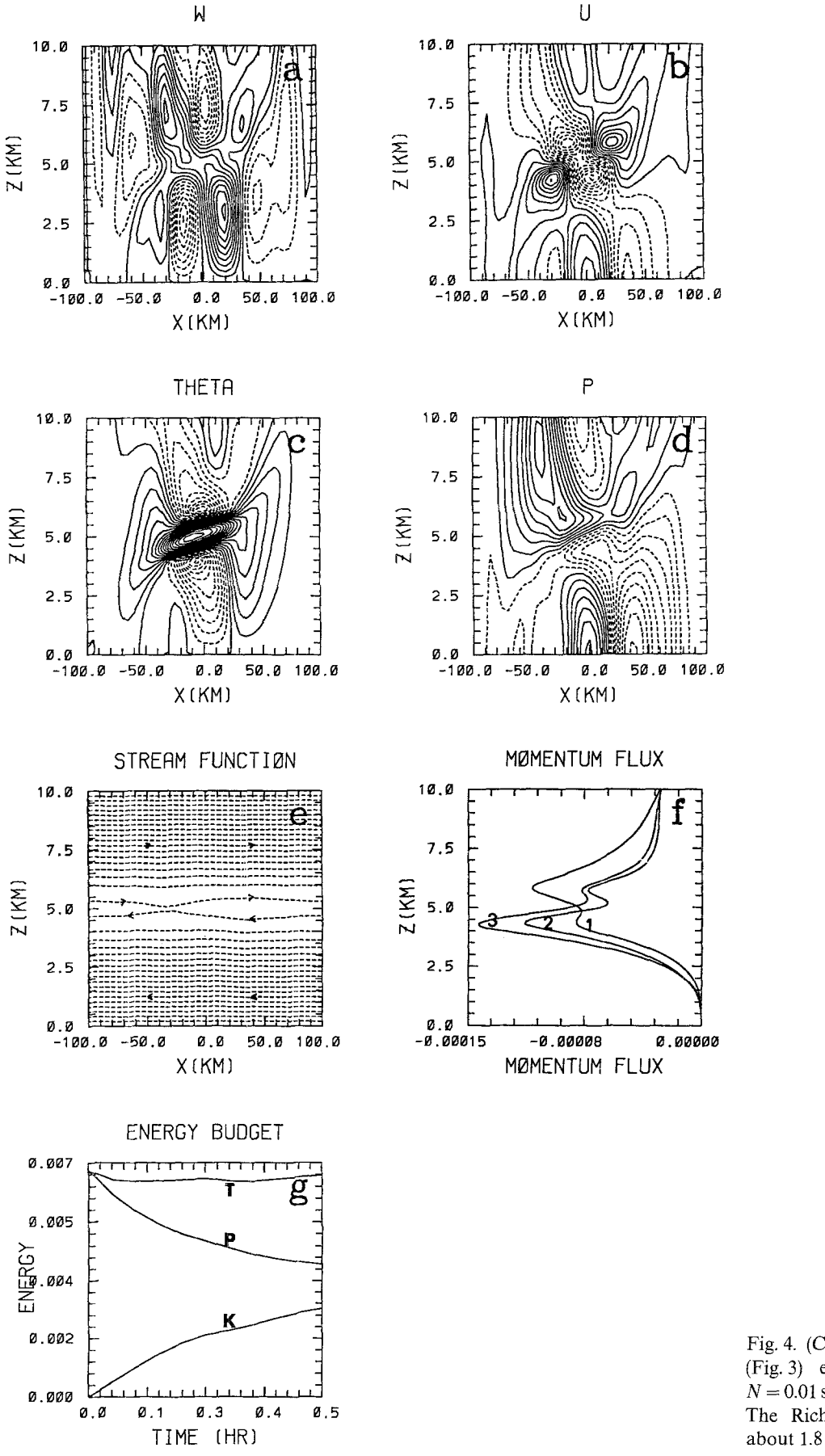

Fig. 4. (Case 1E). Same as Case 1C (Fig. 3) except for a flow with $N = 0.01\,s^{-1}$ after 0.5 h simulation. The Richardson number at z_i is about 1.8

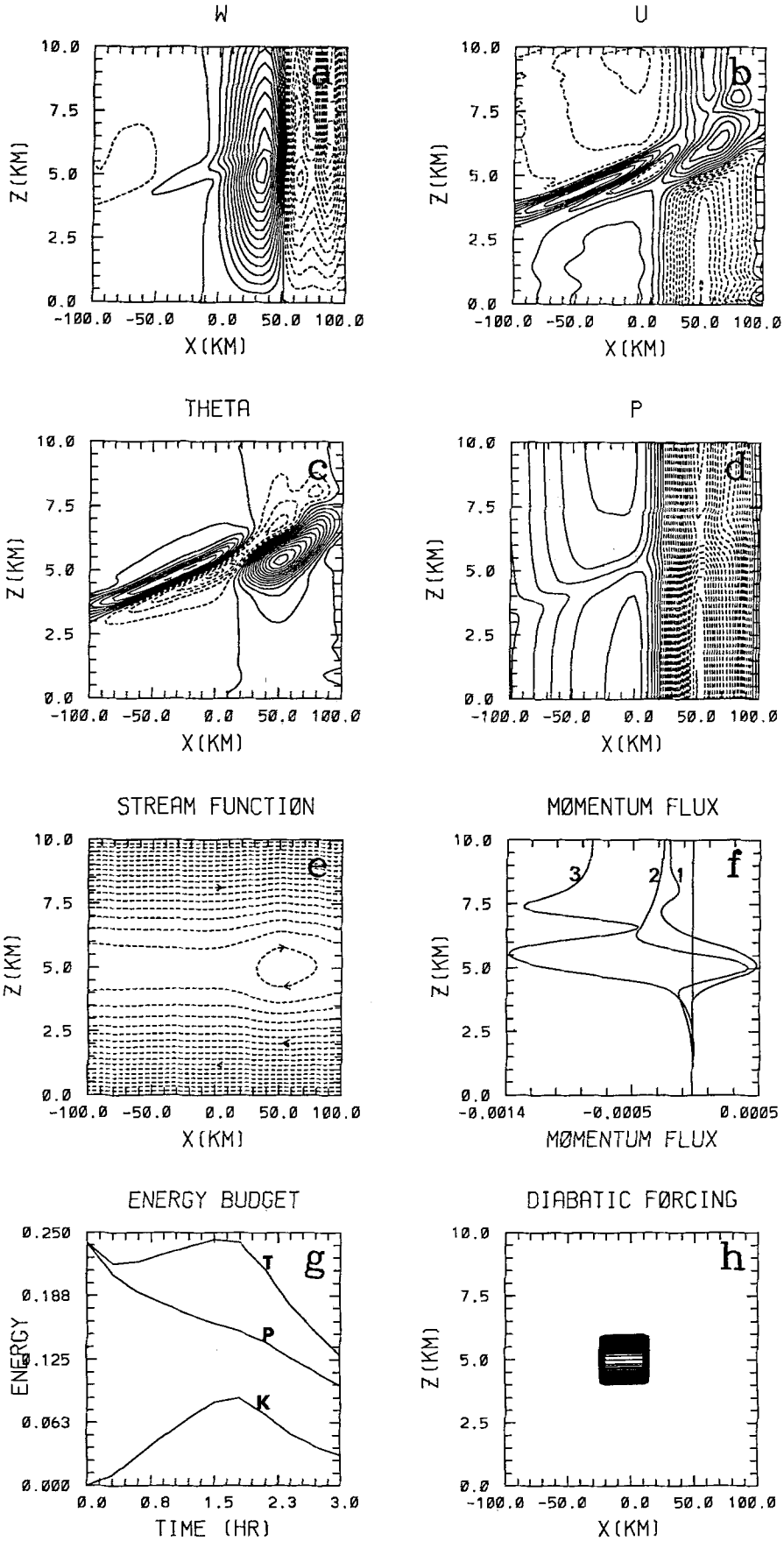

Fig. 5. (Case 2A). Same Case 1C except with a constant shear of $0.0053\,s^{-1}$ centered at 5 km and $N = 0.00168\,s^{-1}$. The Richardson number is 0.1 at every level

(Fig. 5g). A region of very weak downdraft is located at about $x = -60$ km. It appears that these two regions of downward motion are the compensating downdrafts associated with the updraft at the early stage. However, the initial warm region rises to a higher level of about 6.5 km and is advected by the basic wind toward right at that level at the early stage. This is evidenced from the perturbation potential temperature field (Fig. 5c). This also explains the downshear (rightward) movement of both the updraft and downdraft. The compensating downdraft on the downshear (right) side of the updraft can develop much stronger than that on the upshear (left) side since the updraft moves to the downshear side at $t = 3$ h which is already in the decaying stage. Part of the warm air is advected downstream (to the left) in the lower layer below 5 km (Fig. 5b, c, and e). The pressure distribution is similar to Case 1C (Fig. 3d) except it is shifted to the right side of the domain, which is related to the rightward shift of the disturbance. Again, the perturbation surface pressure is roughly equal to the vertical integration of the perturbation potential temperature above. Since the generated vertical and horizontal motions are relatively weak, there is no strong disturbance in the streamfunction field except the overturning region centered at $(x, z) = (50, 5\,\text{km})$. This circulation pattern is similar to that forced by a prescribed steady state heating in a flow with Richardson number greater than 1/4 as solved by Lin (1987) in which the heating is prescribed in a dynamically stabe flow.

The momentum flux profile shows an oscillation in the vertical with the maximum centered at about 6.5 km which is the level of maximum disturbance (Fig. 5f). The vertical momentum flux becomes negative above 7.5 km, which indicates that the energy is able to propagate upward to the stratosphere according to Eliassen and Palm theorem (1960). The positive $\overline{pw}$ at z_T (10 km) and the positive value of the vertical integration of the vertical momentum flux over the whole depth of the physical domain implies that the wave energy is decreasing with time at 2 h, according to Eq. (8). The response at 2 h appears to be a transition stage from a growing stage to a decaying stage, which also can be seen from the time evolution of the wave energy (Fig. 5g). It is interesting to note that the total perturbation wave energy is almost dominated by the potential energy. The kinetic energy makes a minor contribution.

The above result is consistent with linear theories of Orr (1907), Eliassen et al. (1953) and Case (1960). In solving the initial-value problem of a two-dimensional, constant shear flow, they took the Laplace transform in t and Fourier transform in x and then solved the Green's function for the inhomogeneous differential equation. Eliassen et al. found that there exists no discrete modes for $-3/4 < Ri < 1/4$ and the constant shear flow is dynamically stable for $Ri > 0$. Based on an asymptotic solution for long time, Case found that the same result. In addition, an initial perturbation becomes a sum of oscillatory terms plus a term which vanishes as $t^{-1/2}$. With Case's solution in mind, the growing stage in the early time in the present results (Fig. 5g) may be due to the oscillatory behavior. The decaying stage at later times indeed shows a slow decaying rate, although it does not decay exactly as $t^{-1/2}$.

In some numerical simulations of two-dimensional mesoscale convective systems, the importance of a low-level shear has been demonstrated (e.g., Thorpe et al., 1982; Rotunno et al., 1988; Fovell and Ogura, 1989). Specifically, Thorpe et al. have argued that the nonlinear low-level wind profile is responsible for the upshear tilt of a midlatitude squall line. Figure 6 (Case 2C) shows the response of a low-level shear flow after 2 h to an initial temperature perturbation which is confined in a box of $x = -15$ to 15 km and $z = -1$ to 2 km. This initial disturbance corresponds to a warm bubble which is often used in the initiation of a convective cloud in numerical experiments. The low-level shear layer extends from the surface to 4 km with $U_z = 0.0053\,\text{s}^{-1}$. The wind blows toward the left at the surface with a speed of $-10.6\,\text{ms}^{-1}$, reverses its direction at 2 km and stays at a constant speed of $10.6\,\text{ms}^{-1}$. The Brunt-Vaisala frequency is $0.00237\,\text{s}^{-1}$. Thus the Richardson number associated with the basic flow is 0.2.

The vertical field shows the main updraft is located at about $x = -30$ km, with two downdrafts on both sides. There exists no phase tilt in the lower layer below 2.5 km and in the middle layer. It is tilted upstream (left) in the upper layer just below the tropopause as required by the radiation boundary condition. The lack of phase tilt of the main updraft is due to the presence of the

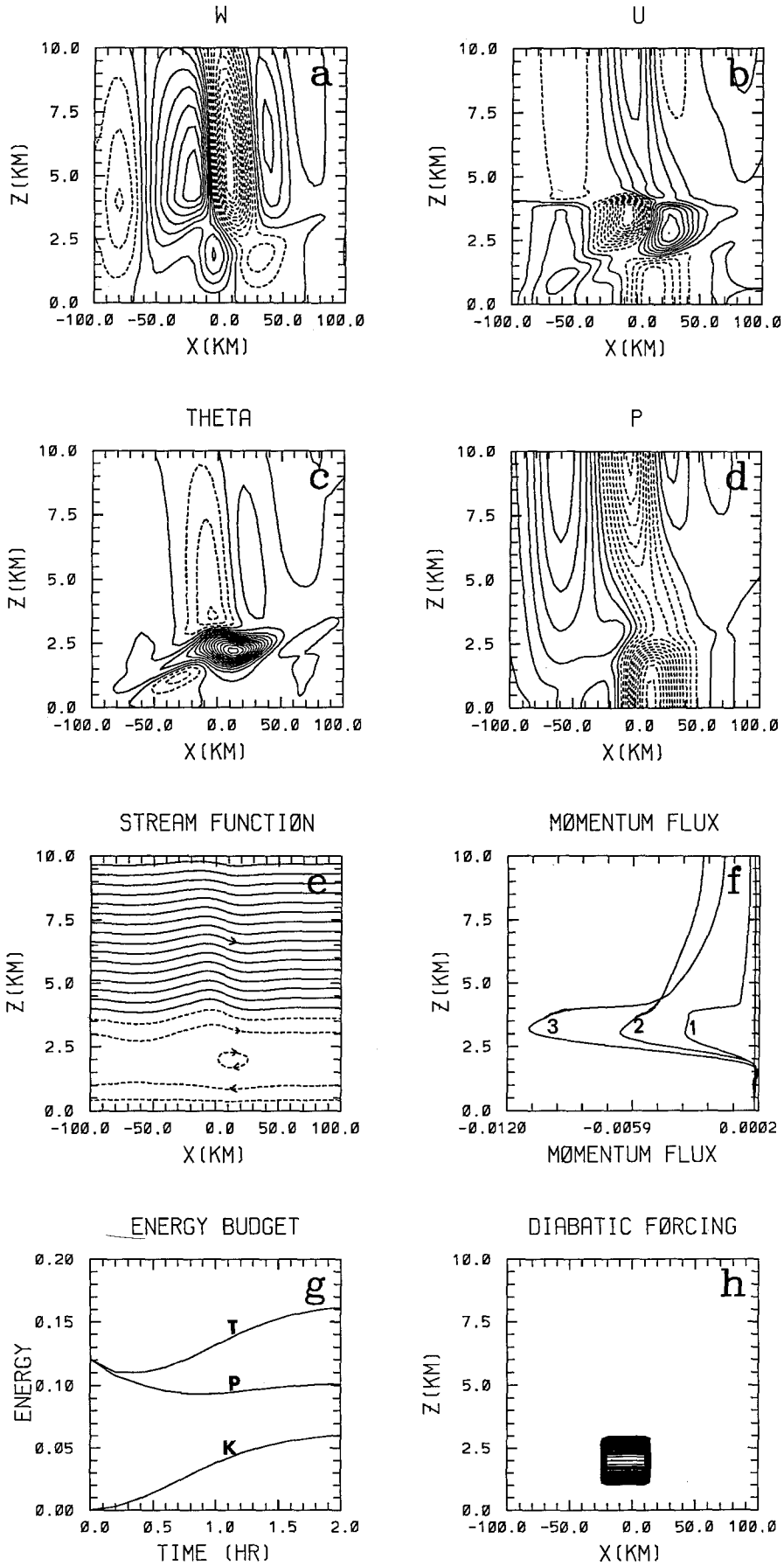

Fig. 6. (Case 2C). The response of a low-level shear flow to an initial temperature perturbation. The low-level shear extends only to 4 km with $U_z = 0.0053\,s^{-1}$ and $U_0 = 10.6\,ms^{-1}$. The wind blows toward the left and reverses its direction at 2 km and then stays constant ($10.6\,ms^{-1}$) above 4 km. The Brunt-Vaisala frequency is $0.00237\,s^{-1}$ below $z = 10$ km and increases linearly to $0.0237\,s^{-1}$ at 15 km. The Richardson number is 0.2. The initial temperature perturbation is confined in a box of $x = -15$ to 15 km and $z = 1$ to 3 km

solid surface which can reflect the wave back (Lin and Smith, 1986). A region of weaker upward motion also forms at $(x, z) = (-5, 1.5\,\text{km})$. This low-level upward motion is associated with a region of convergence (Fig. 6b), which may enhance the development of new convective cells if the air is moist. The θ field (Fig. 6c) indicates that the initial warm bubble rises in the vertical and then is advected by the basic wind, which has a downshear phase tilt. The maximum temperature disturbance is located at $(x, z) = (10, 2.5\,\text{km})$. This region of maximum disturbance forms at a slightly higher level than the initial temperature anomaly since the initial warm air tends to rise. It is then advected by the basic wind which blows toward the right above $z > z_i$ (2 km). There exists a weak cold region above the warm region as required by the mass continuity. This downshear orientation also can be seen from the pertubation horizontal velocity field (Fig. 6b). The pressure perturbation responds to the temperature perturbations directly, as can be seen from Figs. 6c and d. The flow response near the level of wind reversal (Fig. 6e) is similar to the deep shear case (Fig. 5, Case 1E). The vertical momentum flux and evolution of the perturbation wave energy (Figs. 6f and g) are similar to the early stage of the deep shear case (Figs. 5f and g). The perturbation wave energy decreases after 2 h (not shown).

Figure 7 shows a case (Case 2D) similar to Case 2C except the linear low-level shear extends only to 2 km. There exists no basic flow above this level. This type of basic wind profile has often been adopted in numerical simulations of midlatitude squall lines (e.g., Thorpe et al., 1982; Rotunno et al., 1988; Fovell and Ogura, 1989). The vertical motion is similar to the previous case (Case 2C) except with more symmetric gravity waves developed in the layer above the critical level (Fig. 7a). The warm air associated with the initial perturbation stays at the same location (Figs. 7b, c, and e). This also provides evidence for the warm bubble advection argument proposed in Case 2A (Fig. 5). Similar to the previous case, the pressure perturbation responds to the temperature perturbations directly (Figs. 7c and d). A pure gravity wave response in a quiescent fluid is also shown in the streamfunction field (Fig. 7e). The total perturbation energy decreases gradually with time, which indicates that the system is dynamically stable (Fig. 7g).

3.3 Influence of the Solid Lower Boundary

Figure 8 shows a case (Case 3A) similar to Case 1C (Fig. 3) except the inflection point of the basic wind and initial warm air are located at 2 km. Even though the Richardson number is kept the same as 0.1, the response of the flow to the initial perturbation is significantly different from that in Case 1C. It appears that the flow is still dynamically unstable (Figs. 8a, f and g). The disturbance and growth rate are, however, much weaker than those shown in Case 1C. In response to the initial warm bubble, an updraft and two compensating downdrafts are produced. However, this updraft is located at about $x = -35$ km. This is different from what found in Case 1C in which the updraft is located exactly at the original location of the initial perturbation. It is interesting to note that this updraft is propagating against the basic flow in the layer of $z > 2$ km. This response in rather similar to the shallow constant shear case (Case 2C, Fig. 6), which indicates the system is in the transition stage toward a dynamically stable state. This is also evidenced in the time evolution of wave energy (Fig. 8g). Similar to previous cases, the pressure perturbation responds to the temperature perturbations directly (Fig. 8d). The streamfunction shows a region of flow overturning near the inflection level ($z = 2$ km) (Fig. 8e). However, the disturbance is much weaker than that in Case 1C.

Figure 9a shows time evolutions of the perturbation wave energy associated with a hyperbolic tangent basic flow with the inflection point and initial warm air located at 5 km (Case 1C), 4 km, and 2 km (Case 3A) from the model results. The growth rate decreases as the inflection point is moved to a lower level. The results from a linear stability model (LC) also shows the same feature (Fig. 9b). These are consistent with the finding of Einaudi and Lalas (1976) in their theory in which they found that the presence of the solid lower boundary is able to stablize relatively shorter waves in an inviscid stratified shear flow.

4. Concluding Remarks

In this study, nonlinear responses of a dynamically unstable shear flow with critical level to an initial temperature anomaly are investigated using a nonlinear numerical model. Both nonconstant and constant shear profiles of the basic flow

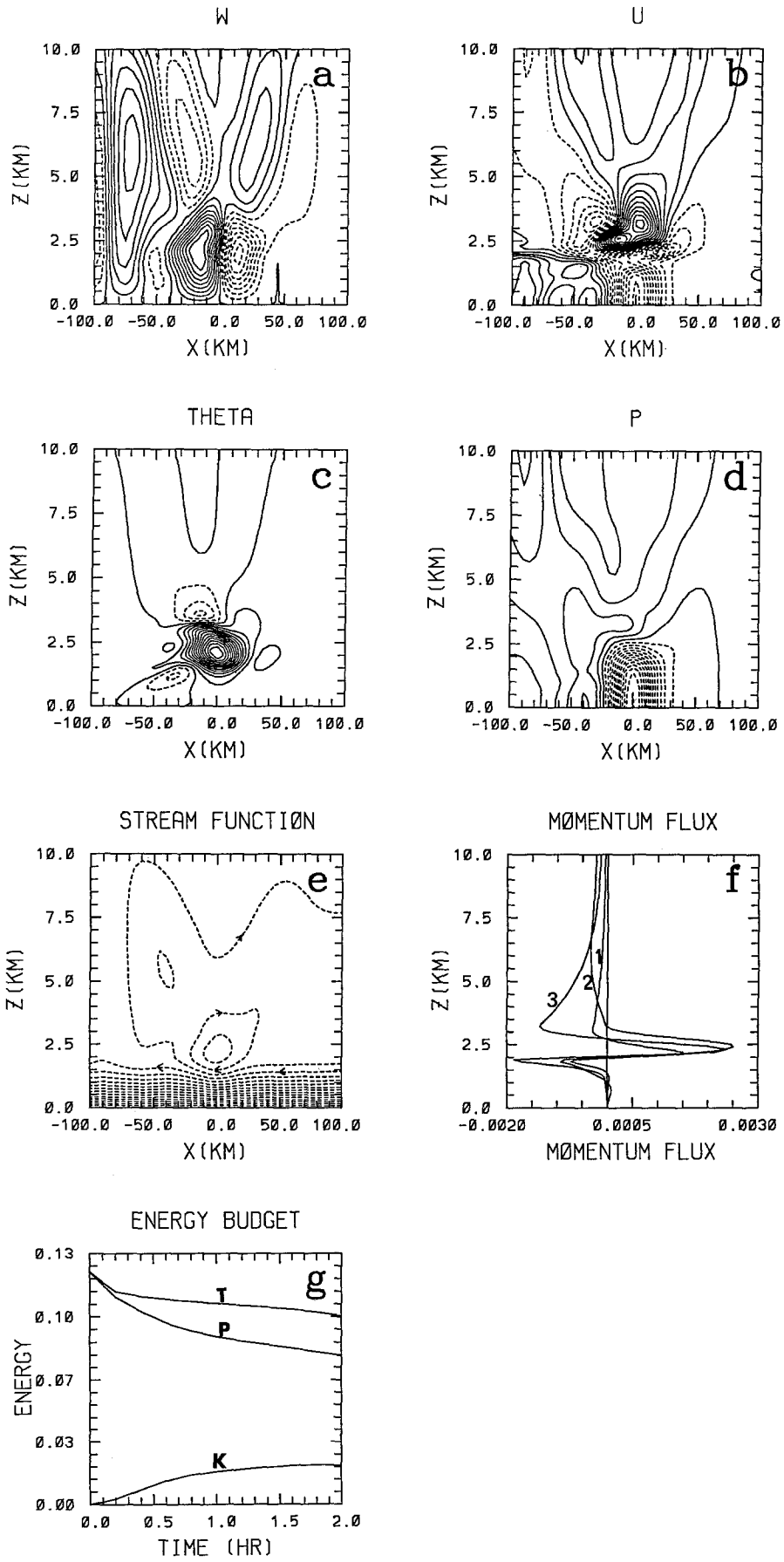

Fig. 7. (Case 2D). Same as Fig. 6 except that the low-level shear only extends to 2 km. There is no basic wind above 2 km

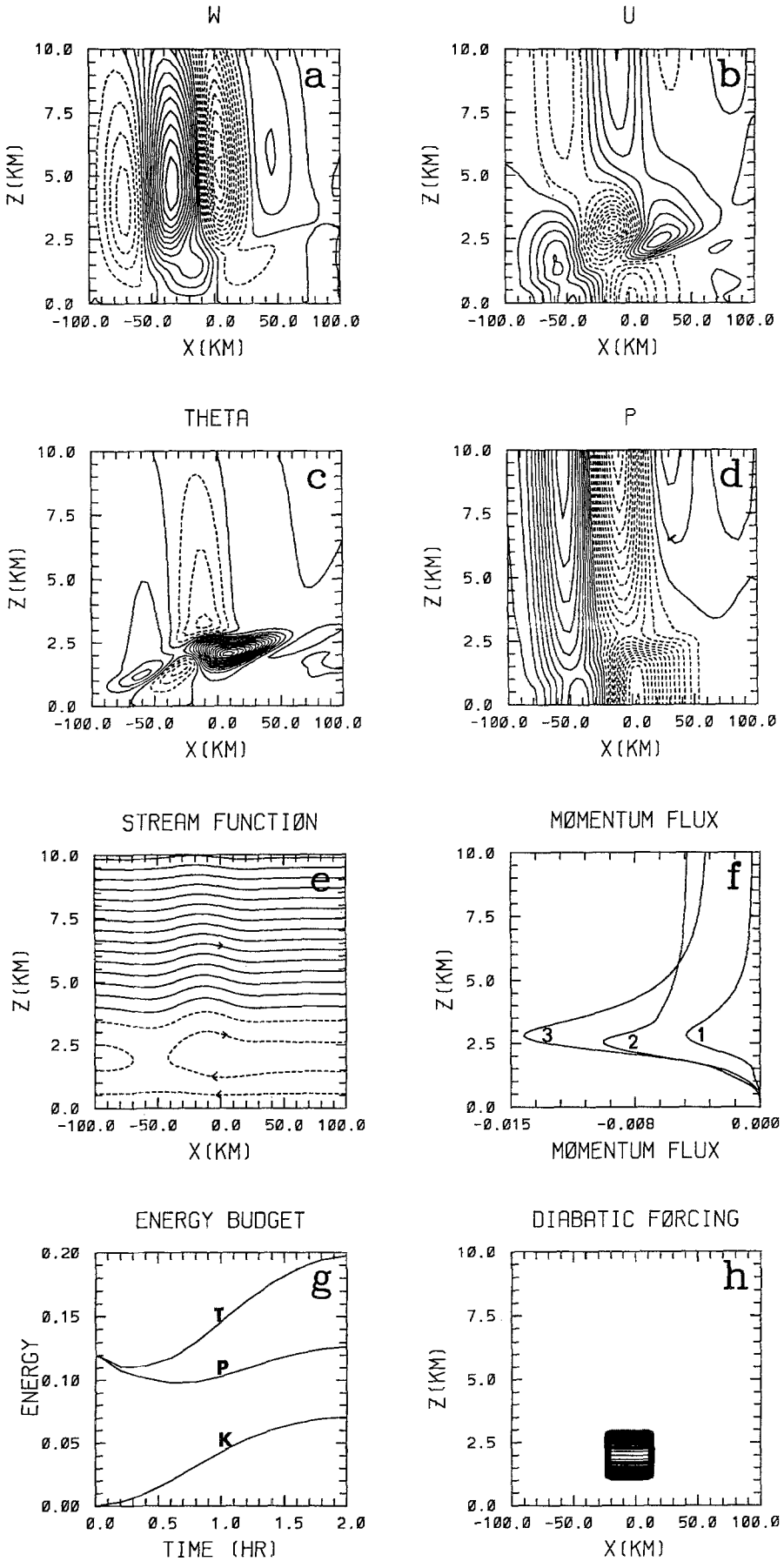

Fig. 8. (Case 3A). Same as Fig. 3 (Case 1C) except the inflection point of the basic wind and initial warm bubble are located at 2 km

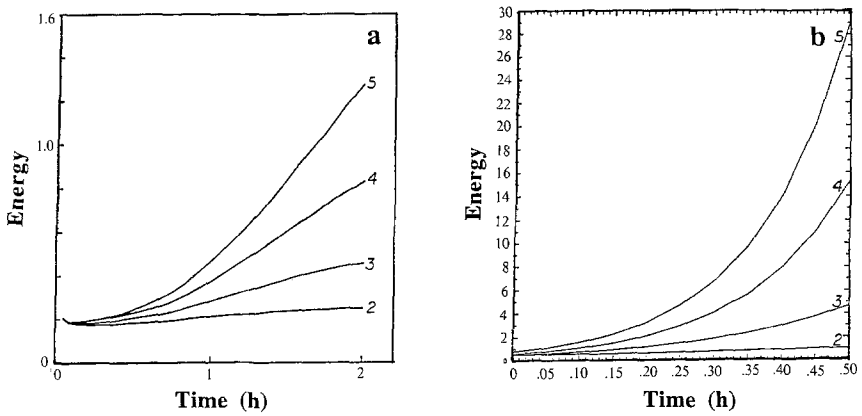

Fig. 9. (a) Time evolutions of the perturbation wave energy associated with a tanh basic flow with the inflection point and initial warm air located at 5 km (curve 5, Case 1C), 4 km (curve 4), 3 km (curve 3), and 2 km (curve 2, Case 3A). (b) Same as (a) except from a linear stability model (after Lin and Chun, 1993)

are considered. Effects of the solid lower boundary on the dynamically unstable, nonlinear flow is also studied.

The findings of this study may be summarized as follows:

- In a dynamically unstable, linear flow with a hyperbolic tangent wind profile, the updraft is tilted upshear. The result is consistent with that of linear stability model (LC). The upshear tilt can be explained by the Orr mechanism (1907) and the energy argument proposed by LC. There exist two separate stages of wave development, a very slow growth during the early stage and a rapid growth during the later stage.
- In a dynamically unstable nonlinear flow, the updrafts produced by a sinusoidal initial temperature anomaly are stronger in the lower layer and are more compact and located further apart compared to the corresponding linear flow. The vertical velocity and horizontal velocity are less in phase. The growth of the disturbance is more rapid at earlier stages compared to the linear response. In addition, the vertical velocity is less in phase with the horizontal velocity in the nonlinear flow. Although, the nonlinearity changes the detailed patterns of the flow, the difference from the linear response is not significant. In fact, the perturbed wave energy is slightly smaller than the linear case.
- For a localized initial temperature perturbation in a dynamically unstable flow, a stronger updraft with two compensating downdrafts is produced. The present study may be applied to investigate the early development of a squall line if one regards the propagation of a squall line as a tropospheric internal gravity wave in a CISK-like process.
- For a constant shear flow with $0 < Ri < 1/4$, the disturbance grows in the early stage and then decays at later times, similar to that found in linear theories of Orr (1907), Eliassen et al. (1953), and Case (1960).
- The influence of the solid lower boundary is to suppress the shear instability in a nonlinear flow with a hyperbolic tangent wind profile of $Ri < 1/4$, similar to the linear theory of Einaudi and Lalas (1976).

Acknowledgments

The author wishes to thank Dr. C.-S. Chen of National Central University, Taiwan and Dr. R. P. Weglarz of North Carolina State University for helpful discussions, and I.-C. Jao for performing the simulations. Valuable comments given by Dr. M. E. Nicholls of the Colorado State University are highly appreciated. This work is supported by the NSF under Grant ATM-88-15780 and Grant ATM-9224595.

References

Bluestein, H. B., Jain, M. H., 1985: Formation of mesoscale lines of precipitation: Severe squall lines in Oklahoma during spring. *J. Atmos. Sci.*, **42**, 1711–1732.

Booker, J. R., Bretherton, F. P., 1967: The critical layer for internal gravity waves in a shear flow. *J. Fluid Mech.*, **27**, 513–539.

Bougeault, P., 1983: A non-reflective upper boundary condition for limited-height hydrostatic models. *Mon. Wea. Rev.*, **111**, 420–429.

Breeding, R. J., 1971: A non-linear investigation of critical levels for internal atmospheric gravity waves. *J. Fluid Mech.*, **50**, 545–563.

Bretherton, F. P., 1966: The propagation of groups of internal gravity waves in a shear flow. *Quart. J. Roy. Meteor. Soc.*, **92**, 466–480.

Bretherton, C., 1988: Group velocity and the linear response of stratified fluids to internal heat or mass sources. *J. Atmos. Sci.*, **45**, 81–93.

Case, K. M., 1960a: Stability of inviscid plane Couette flow. *Phys. Fluids*, **3**, 143–148.

Case, K. M., 1960b: Stability of an idealized atmosphere. I. Discussion of results. *Phys. Fluids*, **3**, 149–154.

Chimonas, G., Einaudi, F., Lalas, D. P., 1980: A wave theory for the onset and initial growth of condensation in the atmosphere. *J. Atmos. Sci.*, **37**, 827–845.

Clark, T. L., Peltier, W. R., 1984: Critical level reflection and the resonant growth of nonlinear mountain waves. *J. Atmos. Sci.*, **41**, 3122–3134.

Cram, J. M., Pielke, R. A., Cotton, W. R., 1992: Numerical simulation and analysis of a prefrontal squall line. Part II: Propagation of the squall line as an internal gravity wave. *J. Atmos. Sci.*, **49**, 209–225.

Crook, N. A., 1988: Trapping of low-level internal gravity waves. *J. Atmos. Sci.*, **45**, 1533–1541.

Drazin, P. G., Reid, W. H., 1981: *Hydrodynamic Stability*. Cambridge: Cambridge University Press, 527 pp.

Einaudi, F., Lalas, D. P., 1976: The effect of boundaries on the stability of inviscid stratified shear flows. *J. Appl. Mech.*, **43**, 243–248.

Eliassen, A., Palm, E., 1960: On the transfer of energy in stationary mountain waves. *Geofys. Publ.*, **22**, 1–23.

Eliassen, A., Hoiland, E., Riis, E., 1953: Two-dimensional perturbations of a flow with constant shear of a stratified fluid. *Inst. Weather Climate Res.*, Oslo, Publ. No. 1.

Farrell, B., 1984: Modal and non-modal baroclinic waves. *J. Atmos. Sci.*, **41**, 668–673.

Fovell, R. O., Ogura, Y., 1989: Effects of vertical wind shear on numerically simulated multicell storm structure. *J. Atmos. Sci.*, **46**, 3144–3176.

Howard, L. N., 1961: Note on a paper of J. W. Miles. *J. Fluid Mech.*, **10**, 509–512.

Klemp, J. B., Lilly, D. K., 1978: Numerical simulation of hydrostatic mountain waves. *J. Atmos. Sci.*, **35**, 78–108.

Klemp, J. B., Durran, D. R., 1983: An upper boundary condition permitting internal gravity wave radiation in numerical mesoscale models. *Mon. Wea. Rev.*, **111**, 430–444.

Lin, Y.-L., 1987: Two-dimensional response of a stably stratified shear flow to diabatic heating. *J. Atmos. Sci.*, **44**, 1375–1393.

Lin, Y.-L., 1994a: Airflow over mesoscale heat sources. Part I: Responses in a uniform flow. Proc. NSC, **18**, 1–32.

Lin, Y.-L., 1994b: Airflow over mesoscale heat sources. Part II: Responses in a shear flow. Proc. NSC, **18**, 119–150.

Lin, Y.-L., Chun, H.-Y., 1991: Effects of diabatic cooling in a shear flow with a critical level. *J. Atmos. Sci.*, **48**, 2476–2491.

Lin, Y.-L., Chun, H.-Y., 1993 (LC): Structures of dynamically unstable shear flows and their implications for shallow internal gravity waves. *Meteorol. Atmos. Phys.*, **52**, 59–68.

Lin, Y.-L., Groff, R. C., 1988: A study of a mesoscale solitary wave in the atmosphere originating near a region of deep convection. *J. Atmos. Sci.*, **45**, 194–205.

Lin, Y.-L., Smith, R. B., 1986: Transient dynamics of airflow near a local heat source. *J. Atmos. Sci.*, **43**, 40–49.

Lin, Y.-L., Wang, T.-A., Weglarz, R. P., 1993: Interactions between gravity waves and cold air outflows in a stably stratified uniform flow. *J. Atmos. Sci.*, **50**, 3790–3816.

Lindzen, R. S., 1988: Instability of plane parallel shear flow. *PAGEOPH*, **126**, 103–121.

Lindzen, R. S., Tung, K. K., 1976: Banded convective activity and ducted gravity waves. *Mon. Wea. Rev.*, **104**, 1602–1617.

Maslowe, S. A., 1972: The generation of clear-air turbulence by nonlinear waves. *Stud. Appl. Math.*, **51**, 1–16.

Maslowe, S. A., 1986: Critical layers in shear flows. *Ann. Rev. Fluid Mech.*, **18**, 405–432.

Miles, J. W., 1961: On the stability of heterogeneous shear flow. *J. Fluid Mech.*, **10**, 496–508.

Moncrieff, M. W., Green, J. S. A., 1972: The propagation and transfer properties of steady convective overturning in shear. *Quart. J. Roy. Meteor. Soc.*, **98**, 336–352.

Nicholls, M. E., Johnson, R. H., Cotton, W. R., 1988: The sensitivity of two-dimensional simulations of tropical squall lines to environmental profiles. J. Atmos. Sci., **45**, 3625–3649.

Nicholls, M. E., Pielke, R. A., Cotton, W. R., 1991a: A two-dimensional numerical investigation of the interaction between sea-breezes and deep convection over the Florida peninsula. *Mon. Wea. Rev.*, **119**, 298–323.

Nicholls, M. E., Pielke, R. A., Cotton, W. R., 1991b: Thermally forced gravity waves in an atmosphere at rest. *J. Atmos. Sci.*, **48**, 1869–1884.

Ogura, Y., Liou, M.-T., 1980: The structure of a midlatitude squall line: A case study. *J. Atmos. Sci.*, **37**, 553–567.

Orlanski, I., 1976: A simple boundary condition for unbounded hyperbolic flow. *J. Compu. Phys.*, **21**, 251–269.

Orr, W. M'F, 1907: The stability or instability of the steady motions of a perfect liquid and of a viscous liquid. Part I: A perfect liquid. *Proc. Roy. Irish Acad.*, **A27**, 9–68.

Pedlosky, J., 1987: *Geophysical Fluid Dynamics*, 2nd edn., New York: Springer, 710 pp.

Phillips, O. M., 1966: *The Dynamics of the Upper Ocean*. Cambridge: Cambridge University Press, 261 pp.

Raymond, D. J., 1984: A wave-CISK model of squall lines. *J. Atmos. Sci.*, **41**, 1946–1958.

Raymond, D. J., 1986: Prescribed heating of a stratified atmosphere as a model for moist convection. *J. Atmos. Sci.*, **43**, 1101–1111.

Rotunno, R., Klemp, J. B., Weisman, M. L., 1988: A theory for strong, long-lived squall lines. *J. Atmos. Sci.*, **45**, 463–485.

Schmidt, J. M., Cotton, W. R., 1990: Interactions between upper and lower atmospheric gravity waves on squall line structure and maintenance. *J. Atmos. Sci.*, **47**, 1205–1222.

Smith, R. B., Lin, Y.-L., 1982: The addition of heat to a stratified airstream with application to the dynamics of orographic rain. *Quart. J. Roy. Meteor. Soc.*, **108**, 353–378.

Stewartson, K., 1981: Marginally stable inviscid flows with critical layers. IMA *J. Appl. Mech.*, **27**, 133–175.

Thorpe, A. J., Miller, M. J., Moncrieff, M. W., 1982: Two-dimensional convection in non-constant shear: A model of mid-latitude squall lines. *Quart. J. Roy. Meteor. Soc.*, **108**, 739–762.

Tripoli, G. L., Cotton, W. R., 1989a: Numerical study of an observed orogenic mesoscale convective system. Part I: Simulated genesis and comparison with observations. *Mon. Wea. Rev.*, **117**, 273–304.

Tripoli, G. L., Cotton, W. R., 1989b: Numerical study of an observed orogenic mesoscale convective system. Part II: Analysis of governing dynamics. *Mon. Wea. Rev.*, **117**, 305–328.

Weglarz, R. P., 1994: Three-dimensional geostrophic adjustment of rotating homogeneous and continuously stratified atmospheres with application to the dynamics of midlatitude jet streaks. Ph.D. dissertation, North Carolina State University, NC, 414 pp.

Yamagata, T., 1976: On trajectories of Rossby wave-packets released in a lateral shear flow. *J. Oceanogr. Soc. Japan*, **32**, 162–168.

Author's address: Yuh-Lang Lin, Department of Marine, Earth, and Atmospheric Sciences, North Carolina State University, Raleigh, North Carolina 27695-8208, U.S.A.